Aircraft conceptual design for optimal environmental performance

R. P. Henderson
Institute for Aerospace Studies
University of Toronto
Ontario, Canada

J. R. R. A. Martins
jrram@umich.edu
Department of Aerospace Engineering, University of Michigan
Michigan, USA

R. E. Perez
Department of Mechanical and Aerospace Engineering
Royal Military College of Canada, Kingston
Ontario, Canada

ABSTRACT

Consideration of the environmental impact of aircraft has become critical in commercial aviation. The continued growth of air traffic has caused increasing demands to reduce aircraft emissions, imposing new constraints on the design and development of future airplane concepts. In this paper, an aircraft design optimisation framework is used to design aircraft that minimise specific environmental metrics. Multidisciplinary design optimisation is used to optimise aircraft by simultaneously considering airframe, engine and mission. The environmental metrics considered in this investigation are CO_2 emissions — which are proportional to fuel burn — and landing-takeoff NO_x emissions. The results are compared to those of an aircraft with minimum direct operating cost. The design variables considered in the optimisation problems include aircraft geometry, engine parameters, and cruise settings. An augmented Lagrangian particle swarm optimiser and a genetic algorithm are used to solve the single objective and multi-objective optimisation problems, respectively.

1.0 INTRODUCTION

Aviation has become a major mode of transportation, accounting for more than 10% of the world's passenger miles traveled[1]. According to the Intergovernmental Panel on Climate Change, it is predicted that civil air transport will continue to grow at a rate of 5% per year[2] . The continued growth in air traffic has caused increasing environmental concerns. Demands by the public, environmentalists, and governments to reduce aircraft environmental impact, have imposed new constraints on the design and development of future aircraft concepts[3]. Some current technological

Paper No. 3712. Manuscript received 4 April 2011, revised version received 26 June 2011, accepted 10 July 2011.

developments in aircraft airframes and engine technologies can reduce the environmental impact of air travel per passenger-mile flown. However, with current technology levels, the net result will still be an absolute increase in global green house gas emissions[2,4]. These emissions will continue to affect the climate, particularly with the expected 5% growth in air transport.

The original concern about aircraft emissions focused on air quality in the vicinity of airports[5], and many efforts have been made towards addressing this issue. However, there are currently additional concerns about the net global warming effects of nitrogen oxides (NO_x) and carbon dioxide (CO_2) emissions, as well as contrails generated from aircraft at cruise altitudes[6]. In spite of uncertainties about the magnitude of the resulting atmospheric effects, many argue that the impact of these emissions on the global atmosphere requires immediate attention because the consequences of not acting could be catastrophic[4].

The motivation for the technological improvements to airframes and engines throughout the history of commercial aviation has been purely economic: by reducing fuel burn, aircraft operating costs were reduced as well. These improvements have been achieved by the development of technologies that increase engine efficiency, reduce airframe drag and structural weight, and streamline air traffic[7-9]. Because of these improvements, fuel burn per passenger-mile has been reduced by more than 70% since the early 1960s[2,7].

Further improvements in efficiency have become increasingly challenging. To develop more efficient aircraft configurations that exhibit minimal environmental impact, the design of the airframe, propulsion system and mission must all be considered simultaneously at the early phases of the design process. The use of numerical optimisation techniques in the design process allows designers to explore different aircraft configurations and to investigate the inherent tradeoffs between aircraft cost and a variety of environmental performance metrics.

Design optimisation is a numerical tool used in many engineering design applications to find the optimal solution to a given design problem. The use of optimisation is of particular importance in aircraft design, where there is a continuous demand to improve performance. Due to the fact that various disciplines are strongly coupled in aircraft design, multidisciplinary design optimisation (MDO) emerged as a field of research that focuses on optimisation techniques that consider the coupling and trade-offs between the various disciplines[10-13]. MDO can thus be used to simultaneously optimise aircraft airframes, engines and missions.

MDO was used for aircraft environmental studies by Antoine and Kroo[14,15]. They used genetic algorithms to optimise aircraft configurations with respect to aircraft noise, NO_x emissions and CO emissions. Multi-objective optimisation was also performed to illustrate the tradeoffs between conflicting objective functions. More recently, Schwartz and Kroo[16] developed a climate model to optimise aircraft for minimum global temperature change. Again, multi-objective optimisation was performed to compare configurations optimised for a variety of environmental metrics. MDO has also been used to develop new aircraft concepts such as blended-wing bodies[17,18] and strut-braced-wing aircraft[19].

In this paper, single and multi-objective optimisations are performed on multiple aircraft to investigate the tradeoffs between the various environmental performance metrics. The metrics of interest include the landing-takeoff (LTO) cycle NO_x emissions, and aircraft mission fuel burn. Note that there are other important metrics that are not considered here, such as noise, manufacturing and disposal. Aircraft optimised for minimum direct operating cost (DOC) are also included for comparison purposes. The design variables include airframe and engine parameters, as well as certain aspects of the aircraft mission. In addition, a large aircraft optimised specifically for shorter ranges is also presented. This type of aircraft would be efficient on heavily used short-range routes.

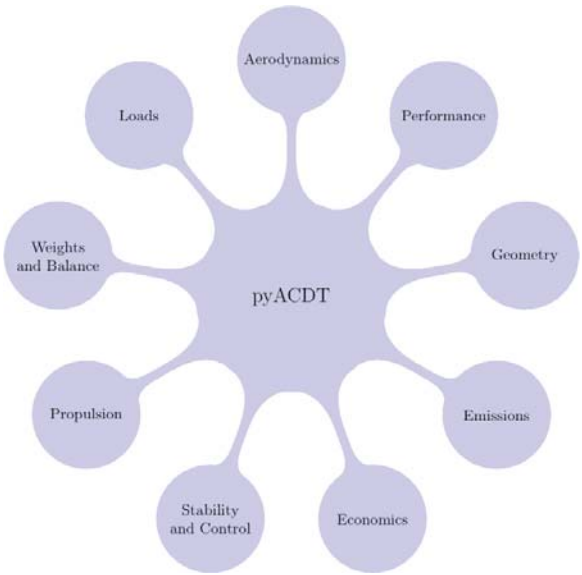

Figure 1. Modules in the Python aircraft conceptual design toolbox (pyACDT).

The aircraft and propulsion conceptual design tools are described in the following section. Results are then presented for narrow- and wide-bodied aircraft optimised for cost and the environmental metrics. The last section summarises the results and conclusions.

2.0 METHODOLOGY

2.1 Aircraft conceptual design

The aircraft conceptual design framework, pyACDT (Python aircraft conceptual design toolbox), consists of a series of modules representing all the major disciplinary analyses needed at the conceptual design stage[20]. The framework uses object-oriented concepts to represent the models of the aircraft components, engine components, mission-dependent characteristics, and disciplinary analyses. Figure 1 illustrates the disciplines integrated into pyACDT that are considered in this study.

To provide rapid execution and robustness, low- to medium-fidelity analyses are used in each of these disciplinary modules. The design of the framework makes it easy to change the design variables, constraints, objective functions and disciplinary analyses. The details of each discipline are described below.

2.1.1 Geometry

This module defines the geometry of the aircraft configuration. Certain parameters are set based on the type of aircraft being modelled. The dimensions of the fuselage and seating arrangements are defined, all lifting surfaces are created, and the overall arrangement of the aircraft is determined. A generic parametric constructive geometry modeler is used to create all aircraft component outer-mold-lines, as shown in Fig. 2.

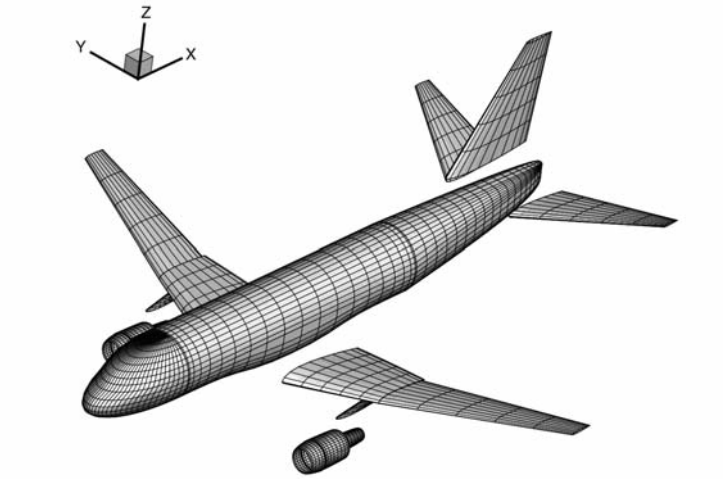

Figure 2. Aircraft parametric geometry model.

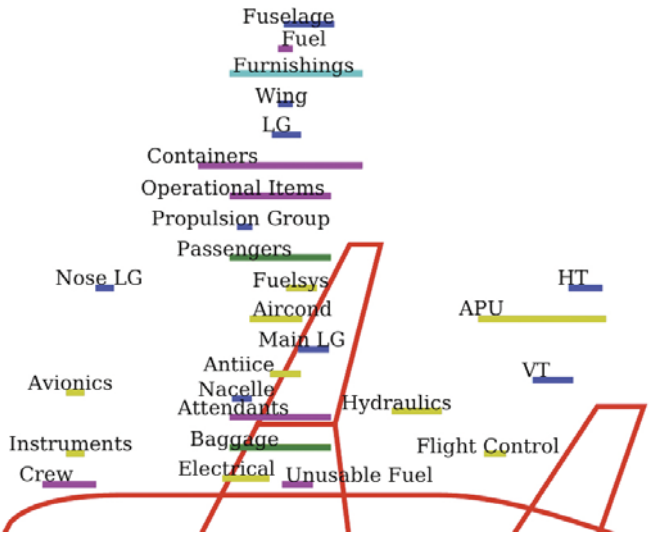

Figure 3. Centre of gravity limits for major aircraft components.

The aircraft layout is defined using hierarchical component decomposition with association between components that are connected. The geometry of each aircraft component is derived from a set of primary physical attributes and any other additional geometric parameters specific to the component. The geometry module has been designed to allow rapid generation of any aircraft configuration, ranging from conventional configurations to nonplanar wings and blended-wing bodies. However, pyACDT is currently limited to the analysis of conventional aircraft configurations due to the empirical nature of certain disciplinary analyses included in the framework.

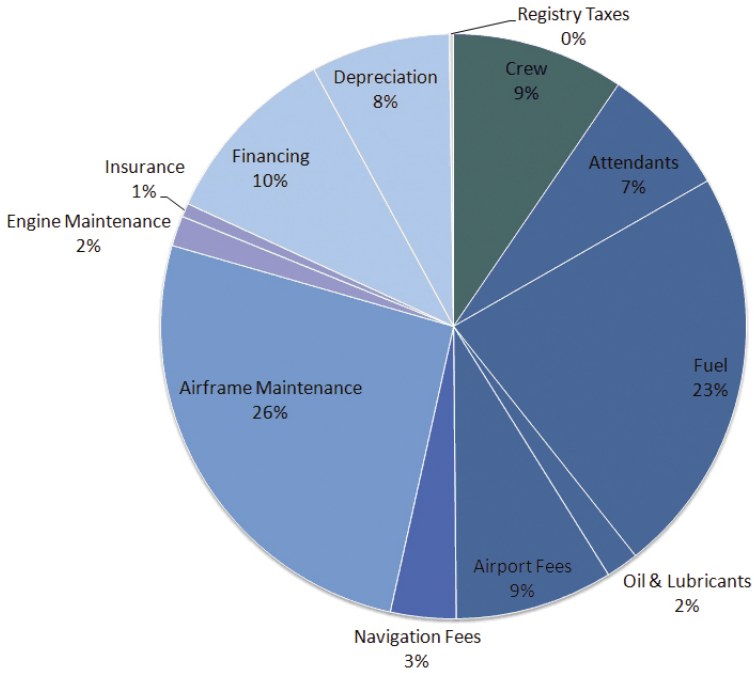

Figure 4. Direct operating cost breakdown.

2.1.2 Weights and balance

The aircraft take-off weight is calculated iteratively by adding the component weights, which are estimated using statistical models[21-23], and the fuel required for the mission. The maximum permissible centre of gravity (CG) range for the configuration is calculated from each aircraft component's CG range based on its own geometry, and physical and functional considerations[24]. Figure 3 illustrates typical component CG ranges for a conventional aircraft configuration.

2.1.3 Cost

The cost analysis has the ability to produce total life cycle cost estimates for different aircraft configurations by calculating the research and development, production, and end-of-life-cycle costs for the airframe, engine, and systems, as well as the direct and indirect operating cost of the airplane. The empirical methods used to predict the various costs are only valid for conventional tube and wing configurations. For the purposes of this paper, only the direct operating cost (DOC) is calculated. DOC is typically used as a figure of merit for aircraft design trade studies and is expressed as the cost per passenger-mile flown. There are typically two components associated with the DOC of aircraft. The DOC cash component represents the cost of operating the aircraft in scheduled service, and includes flights and cabin crew wages, engine and airframe maintenance, fuel and oil costs, navigation fees, and airport landing fees. The other component of DOC consists of capital costs, which must be accounted for over the life of the aircraft, but which are usually allocated on a yearly basis to the operation of the aircraft. The capital costs include insurance, interest and depreciation[25]. Figure 4 illustrates an example of the cost breakdown for a typical airliner.

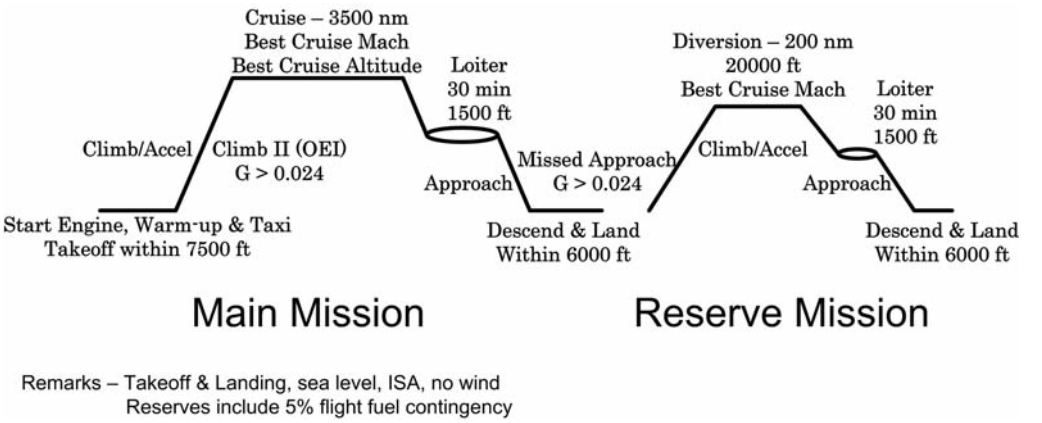

Figure 5. Typical airliner mission profile.

2.1.4 Performance

Given a mission profile, the performance module estimates mission fuel burn as well as point performance parameters. A typical airliner mission profile is illustrated in Fig. 5.

The performance parameters of interest include takeoff field length, landing field length and second segment climb gradient. The cruise range is calculated based on the Breguet range equation. The parameters used in this equation are averaged based on the initial and final cruise values. The fuel burned during the secondary mission segments is based on fractions of the aircraft maximum takeoff weight. The additional fuel required to climb is a function of the initial cruise altitude and maximum take-off weight. Throughout the mission profile, additional aerodynamic and propulsive parameters are calculated and used to evaluate constraints in the optimisation problems. These parameters include wing and tail total lift, maximum lift coefficients, thrust-to-drag ratios, static margins and angles-of-attack.

2.1.5 Aerodynamics

Aircraft lift and drag are calculated based on low- to medium-fidelity models appropriate for the conceptual design stage. The lift-induced drag is computed using a potential flow panel method[26], which can be employed for a wide range of nonplanar lifting surface configurations. A typical aerodynamic model using this method is shown in Fig. 6, which shows the wing surface discretisation and the horseshoe vortices.

An aerofoil analysis code is used within the panel method to model lift surface camber effects and for maximum lift coefficient calculations. The parasite drag is calculated using a detailed component build-up method[22], which takes into consideration viscous separation and mutual interference effects between components. Transonic wave drag is modeled based on Lock's empirical approximation, using the Korn equation extended by Mason to include sweep[12]. The maximum lift coefficients for the takeoff and landing configurations are calculated by estimating the changes in maximum lift coefficient due to the deployment of leading-edge slats and trailing-edge flaps, and adding these changes to the clean configuration maximum lift coefficient. The estimated changes in maximum lift coefficient are based on the Engineering Sciences Data Unit methods[27-30], with approximations from March[31].

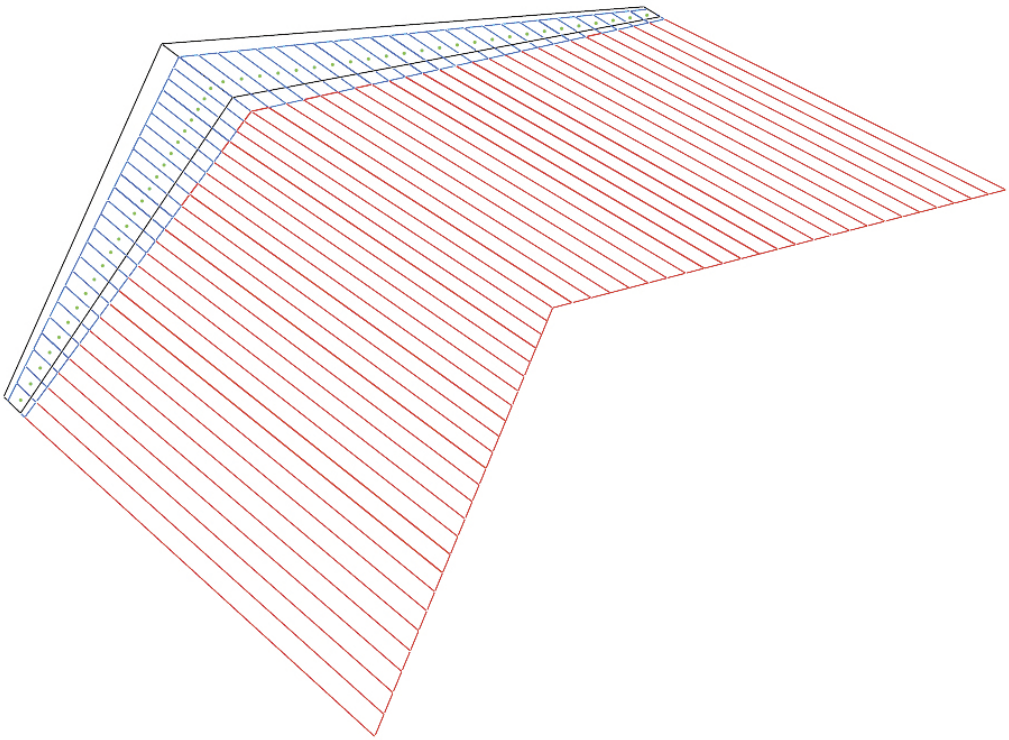

Figure 6. Aerodynamic model showing wing surface discretisation and horseshoe vortices.

2.1.6 Stability

The stability module uses the panel method to compute aircraft longitudinal static stability at all flight conditions. The aircraft is first trimmed and then the static margin is computed for the trimmed condition, by performing a finite difference to estimate the moment coefficient derivative with respect to the lift coefficient.

2.1.7 Propulsion

The propulsion module can estimate performance parameters — primarily thrust and fuel consumption — for various engine configurations. For the optimisation problems considered in this study, a two-spool separate exhaust turbofan engine model was used, as illustrated in Fig. 7.

The model predicts the performance using classical steady zero-dimensional thermodynamic analyses. The engine design point is first determined by running the propulsion code at sea-level static (SLS) conditions, for the given values of the engine design variables. Then, turbomachinery maps representative of aircraft compressors and turbines are scaled to the design point. This scaling places the maps in line with the current design point so that off-design analysis can be performed. The propulsion code can then be run for the various off-design conditions required by the emissions and performance modules. The off-design condition can correspond to a change in alti-

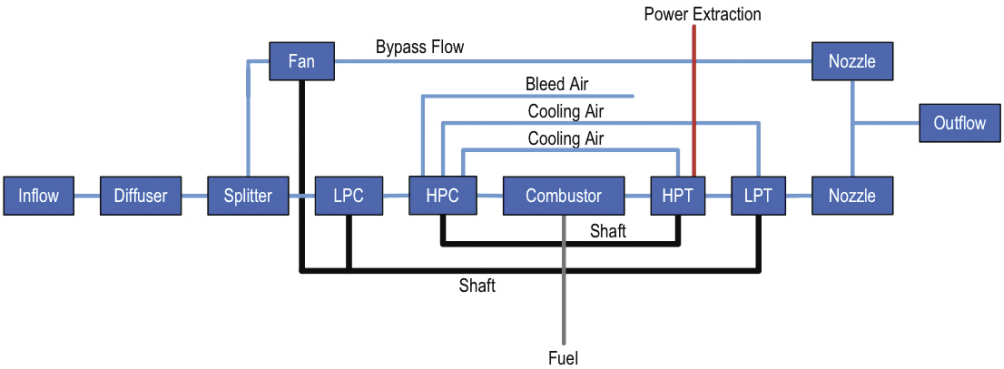

Figure 7. Two-spool separate exhaust turbofan engine model.

tude, Mach number, or both. The off-design code is simply run until convergence to a specified throttle setting. When a specific thrust is required at an off-cycle point — e.g. matching thrust and drag at cruise — the cycle is solved with a controller that ensures that the target thrust is achieved. More details on this model can be found in previous work by the first author[32].

In all cases, global parameters such as thrust and thrust-specific fuel consumption are calculated. Thermodynamic properties for each engine component are also stored; these are critical for the emissions module, where specific component properties are required in the analyses.

2.1.8 Emissions

The emissions module focuses on calculating the total mission CO_2 and the landing-takeoff (LTO) cycle NO_X emissions. The emissions are directly proportional to the amount of fuel burned. Therefore, the emissions for the complete mission can be computed by multiplying the fuel-specific emission index (EI), the fuel flow ($\dot{m}$), and the flight time (Δt) for each segment i and adding them as follows,

$$MissionEmissions = \sum_{i=1}^{N} EI_i \times \dot{m}_i \times \Delta t_i, \qquad \ldots (1)$$

where N is the total number of segments.

For CO_2 emissions, we use a constant EI of 3·149kg of emissions per kg of fuel burned[14]. The EI for NO_x is dependent on the thrust setting and can be predicted using a correlation that depends on the flow conditions both downstream and upstream of the combustor[33,34]. The correlation is given by

$$EI_{NO_x} = 0{\cdot}004194 T_4 \left(\frac{P_3}{439}\right)^{0{\cdot}37} \exp\left(\frac{T_3 - 1471}{345}\right), \qquad \ldots (2)$$

where P_3 is the combustor entrance absolute pressure in psi, and T_3 and T_4 are the entrance and exit combustor temperatures, respectively, in Rankine.

The computation for the LTO cycle follows the International Civil Aviation Organization (ICAO) emissions regulations for civil subsonic turbofan engines over an operational cycle around airports. This LTO cycle is representative of a typical commercial aircraft operation as it

Table 1
ICAO landing-takeoff cycle

Mode	Thrust setting (% max SLS)	Time (min)
Take-off	100·0	0·7
Climb out	85·0	2·2
Approach	30·0	4·0
Idle	7·0	26·0

descends from 3,000ft on its approach path to the time it attains the same altitude during take-off[35] and is detailed in Table 1.

2.2 Optimisation methods

Two optimisation methods are currently used in the framework. For single objective optimisations, a parallel augmented Lagrangian particle swarm optimisation (ALPSO) algorithm is used[36]. This is an algorithm based on particle swarm optimisation, which is a gradient-free population-based optimisation method for unconstrained problems. ALPSO handles the constraints by using an augmented Lagrangian approach[37]. A parallel multi-objective genetic algorithm — another gradient-free population-based optimisation method — is used to investigate the tradeoffs between the objective functions considered throughout this work[38].

2.3 Problem definition

The goal of the MDO problems presented in this section is to find optimal aircraft configurations based on a variety of metrics. Typically, aircraft are designed with economics as the driver, and therefore, aircraft optimised for minimum direct operating cost are also presented; this allows for a direct comparison between aircraft optimised for various environmental metrics and aircraft as they are currently designed. The environmental objective functions to be minimised in the present work are fuel burn — a surrogate for CO_2 emissions — and LTO cycle NO_x emissions. The optimisation problems are focused on the design of a narrow-body airliner and a larger wide-body aircraft, both with twin wing-mounted turbofan engines and a conventional aft tail.

The design variables in the optimisations include airframe, engine and mission parameters. Most of these design variables are related to the wing geometry, the propulsion system thermodynamic cycle, and the cruise mission segment. The design variables and their respective bounds are listed in Table 2. The design variable bounds for the larger wide-body aircraft, when different from the narrow-body aircraft values, are indicated in brackets. Note that the cruise Mach number is one of the design variables. As we will see, this is a significant variable in the trade-off between emissions and cost.

A variety of constraints are imposed in the optimisation problems, all of which are listed in Table 3. These constraints ensure that the optimised aircraft meet certain performance, aerodynamic, stability and geometrical requirements. The geometric constraints include wing span and available wing fuel volume. The performance constraints include takeoff and landing field lengths, and engine-out climb gradients. Aerodynamic constraints are imposed on the wing and tail lift coefficients at various flight phases to avoid stall, and on the cruise angle of the fuselage for passenger comfort. Constraints are also imposed on the engine to ensure that the thermodynamic properties are physically achievable, and that there is a sufficient thrust margin at all flight

Table 2
Design variables and bounds for the narrow- and wide-body configurations
(bound values for the wide-body are shown in brackets)

Variable	Lower bound	Upper bound
Maximum takeoff weight (lb)	100,000 [200,000]	250,000 [500,000]
Wing span (ft)	60	260
Wing root chord (ft)	5 [10]	30 [60]
Wing taper ratio	0·1	1·0
Wing leading edge sweep (deg)	0	50
Wing root thickness-to-chord ratio	0·08	0·25
Wing tip thickness-to-chord ratio	0·08	0·25
Wing location along fuselage	0·2	0·5
Horizontal tail area (ft)	200	800 [1000]
Horizontal tail leading edge sweep (deg)	0	50
Horizontal tail thickness-to-chord ratio	0·07	0·11
Vertical tail area (ft)	150	600 [900]
Engine takeoff thrust (lb)	12,000	90,000
Engine bypass ratio	4	15
Engine fan pressure ratio	1·5	2·0
Engine LPC pressure ratio	3·5	4·0
Engine HPC pressure ratio	9·0	15·0
Engine turbine inlet temperature (R)	3,000	3,500
Cruise Mach number	0·4	0·9
Initial cruise altitude (ft)	15,000	45,000
Final cruise altitude (ft)	15,000	45,000

Table 3
Optimisation problem constraints

Constraint	Value
Wing span (ft)	≤ 260
Wing leading edge sweep	≤ Horizontal tail leading edge sweep
Wing tip thickness-to-chord ratio	≤ Wing root thickness-to-chord ratio
Wing fuel volume	≥ Required block fuel volume
Forward CG position (% MAC)	≥ 0·05
Aft CG position (% MAC)	≤ 0·55
Takeoff field length (ft)	≤ Specified takeoff field length
Tail rotation lift coefficient	≤ Tail maximum lift coefficient
Engine-out climb gradient	≥ FAR climb gradient requirement
Range	= Specified range
Landing field length	≤ Specified landing field length
Angle of fuselage at cruise (deg)	≤ 2·5
Drag-to-thrust ratio	≤ 0·88
Static margin	≥ 0·2
Horizontal tail area	= Area determined by tail volume coefficient
Vertical tail area	= Area determined by tail volume coefficient

Table 4
Constant parameters in narrow-body optimisation problems

Variable	Value
Range (nm)	2,900
Passengers	108
Flight crew	2
Flight attendants	5
Takeoff field length (ft)	7,500
Landing field length (ft)	6,000

phases. Longitudinal static stability is also enforced throughout the mission by evaluating and constraining the static margin at all flight phases. Tail volume coefficients are also constrained to ensure lateral stability.

3.0 RESULTS

3.1 Narrow-body aircraft

The narrow-body configuration is a 108-passenger aircraft with a relatively short range of 2,900nm, which is typical for transcontinental flights. Table 4 lists some of the major specifications that define this type of aircraft. These parameters are held constant for all optimisation cases, unless specified otherwise. The aircraft is first optimised for minimum cost, minimum LTO cycle NO_X emissions and minimum mission fuel burn for a fixed range. Then, the range is added as a design variable and the fuel burn per distance flown is minimised. Finally, Pareto optimal results are generated for cost and fuel burn.

3.1.1 Single objective environmental optimisations

In this section we perform single objective optimisations for minimum DOC, minimum mission fuel burn and minimum LTO NO_X emissions. The results for minimum DOC are based on a fuel price of US$1·50 per gallon. Table 5 lists the optimal design variable values for each configuration, as well as additional performance parameters. A planform view of each configuration is shown in Fig. 8.

As shown in Table 5, the aircraft optimised for minimum DOC has a 24·1% and 40·0% lower cost when compared to the minimum fuel burn and minimum NO_X aircraft, respectively. For a smaller aircraft such as this one, the impact of fuel cost on DOC is not as high as for larger aircraft, and therefore, the minimum DOC aircraft cruises at a high subsonic speed to reduce flight block time. In order to fly at this cruise speed, this aircraft has highly swept wings and thin aerofoils, and flies at a low cruise lift coefficient. These design choices permit the aircraft to fly at high Mach numbers without a prohibitive rise in transonic wave drag. However, this aircraft does have a large penalty in aerodynamic efficiency and therefore requires more fuel to achieve the same cruise range. Since fuel does have an impact on operating cost, this aircraft is designed with high-efficiency engines. The bypass ratio is smaller than that of the minimum fuel burn aircraft, due to the high thrust required to match the high cruise drag. A high thrust-to-weight ratio is required to meet the takeoff field length and second segment climb gradient requirements as well. Since

Table 5
Optimal narrow-body configurations for the three objectives

Objective	DOC	Fuel burn	LTO NO_x
Maximum takeoff weight (lb)	119,600	129,900	125,900
Wing reference area (ft)	994·6	1520·3	1759·4
Wing aspect ratio	5·73	16·38	17·25
Wing taper ratio	0·192	0·317	0·38
Wing span (ft)	75·5	157·8	174·2
Wing leading edge sweep (deg)	49·5	8·1	6·4
Wing root thickness-to-chord ratio	0.153	0.25	0·25
Wing tip thickness-to-chord ratio	0.12	0.143	0.249
Wing location along fuselage	0·221	0·377	0.4122
Horizontal tail area (ft)	252·7	290·5	373·9
Horizontal tail leading edge sweep (deg)	49·97	35·5	20·0
Horizontal tail thickness-to-chord ratio	0·0969	0·103	0·097
Vertical tail area (ft)	171·0	303·0	406·4
Engine takeoff thrust (lb)	20,950	23,555	12,240
Engine bypass ratio	8·895	12·69	12·98
Engine fan pressure ratio	1·704	1·5	1·4
Engine LPC pressure ratio	3·737	4·0	3·5
Engine HPC pressure ratio	15·0	14·86	9·0
Engine turbine inlet temperature (R)	3,462	3,500	3,100
Cruise Mach number	0·90	0·61	0·42
Initial cruise altitude (ft)	32,200	33,490	15,020
Final cruise altitude (ft)	38,570	36,310	19,710
Direct operating cost (USD)	31,409	41,502	52,471
Fuel burn (lb)	25,230	21,334	24,615
Block time (h)	6·33	8·96	12·0
LTO NO (lb)	18·16	19·56	3·16
Wing loading (lb/ft)	120·2	85·5	71·56
Thrust-to-weight ratio	0·35	0·365	0·194
Average cruise lift-to-drag ratio	14·14	20·95	20·5
Average cruise thrust-specific fuel consumption (lb/lbf·h)	0·54	0·395	0·37
Average cruise speed (kt)	520·8	352·2	257·8

the span and the aspect ratio of this aircraft are quite small, the induced drag is high, and therefore this aircraft requires high thrust at low speeds. The span of this aircraft is low to offset the increase in wing weight caused by the high sweep.

The aircraft designed for minimum fuel burn requires 10·4% and 10·0% less fuel when compared to the aircraft designed for minimum cost and minimum LTO NO_x, respectively. This aircraft achieves better fuel efficiency via high aerodynamic efficiency and fuel efficient high-bypass ratio engines. The aerodynamic efficiency is due to the high aspect ratio wing, which reduces the induced drag. Because the aircraft flies at a lower cruise Mach number, the wing loading is low relative to the minimum cost design. The aircraft easily meets the takeoff field length and second segment climb gradient constraints because of its larger wing area and high thrust-to-weight ratio.

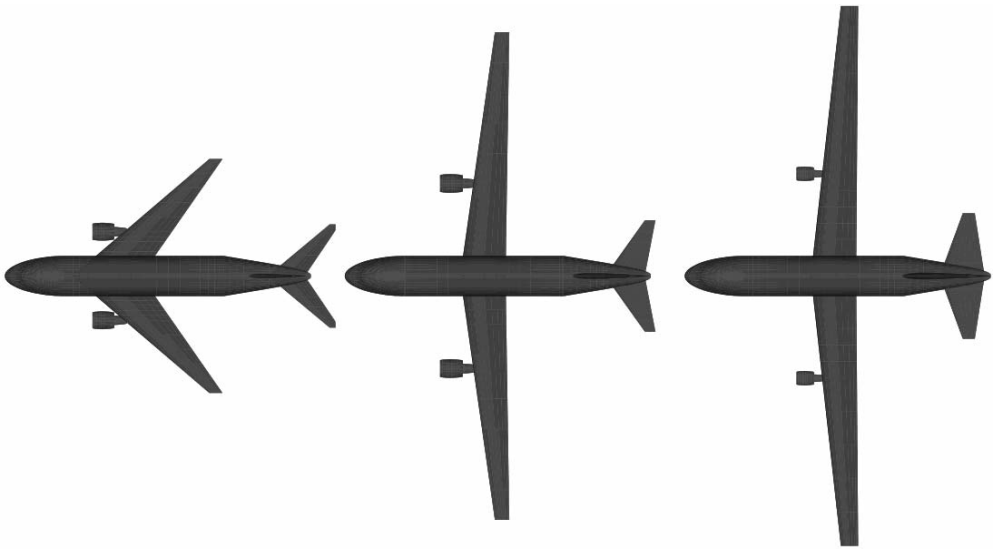

Figure 8. Narrow-body aircraft optimised for: DOC (left), fuel burn (centre), LTO NO_X (right).

As mentioned previously, however, the cost of operating this slower aircraft is much higher than the cost associated with the minimum cost aircraft because of the longer block time.

The aircraft designed for minimum LTO NO_X has 82·6% and 83·8% lower NO_X emissions when compared to the aircraft designed for minimum cost and minimum fuel burn, respectively. This aircraft achieves these reductions with low-thrust, high-bypass ratio engines operating at low temperatures and pressures. The low thrust engine combined with a high-bypass ratio decreases the fuel flow in the engine core. The decrease in pressures and temperatures reduces the NO_X emissions index. Therefore, the low emissions index combined with a low core mass flow rate drastically reduces the NO_X output. Because of this, however, the aircraft costs much more to operate than the minimum cost aircraft and burns more fuel than the minimum fuel burn aircraft. Because the engines are extremely small with high-bypass ratios, this aircraft must fly at low speeds and low altitudes to produce enough thrust to match the cruise drag. The cruise altitudes are also much lower to help maintain cruise lift coefficients at reasonable values at the low cruise speed. The wing area is large for similar reasons. Because the engines have poor fuel efficiency, the aircraft has to achieve a high aerodynamic efficiency during cruise to meet the range requirement. For this reason, its average cruise lift-to-drag ratio is similar to the minimum fuel burn aircraft. Because the engines for the minimum LTO NO_X emissions aircraft are so small, the second segment climb gradient is an active constraint. The engines are made as small as possible, while still achieving the required climb gradient.

3.1.2 Design range optimisation

In the optimisations performed so far, the mission range was a constraint, since range is usually a design specification. However, the fuel burn per passenger per distance flow depends on the mission range. In this design range optimisation study, the fuel burn per passenger per distance flown is minimised with respect to the range, and with respect to the design variables listed in Table 2. For short ranges, the fuel burn per distance flown is dominated by the fuel expended during

Table 6
Narrow-body results for maximum fuel-payload efficiency

	Variable cruise Mach	Fixed cruise Mach
Maximum takeoff weight (lb)	135,300	125,40
Wing reference area (ft)	1,497·1	1,094
Wing aspect ratio	18·12	11·4
Wing taper ratio	0·3	0·1
Wing span (ft)	164·7	111·7
Wing leading edge sweep (deg)	0·0	36·1
Wing root thickness-to-chord ratio	0·188	0·1
Wing tip thickness-to-chord ratio	0·182	0·12
Wing location along fuselage	0·435	0·289
Horizontal tail area (ft)	266·9	231·0
Horizontal tail leading edge sweep (deg)	35·75	50·0
Horizontal tail thickness-to-chord ratio	0·106	0·11
Vertical tail area (ft)	325·6	207·1
Engine takeoff thrust (lb)	22,770	23,710
Engine bypass ratio	11·66	9·85
Engine fan pressure ratio	1·544	1·556
Engine LPC pressure ratio	4·0	3·894
Engine HPC pressure ratio	15·0	14·76
Engine turbine inlet temperature (R)	3,496	3,390
Cruise Mach number	0·64	0·76
Initial cruise altitude (ft)	35,050	35,150
Final cruise altitude (ft)	38,700	39,280
Fuel (lb)	31,595	29,441
Block time (h)	10·39	7·72
Range (nm)	3,433	3,040
Fuel burn per distance (lb/nm)	7·27	7·66
Wing loading (lb/ft)	90·38	114·6
Thrust-to-weight ratio	0·337	0·378
Average cruise lift-to-drag ratio	21·6	18·03
Average cruise thrust-specific fuel consumption (lb/lbf·h)	0·41	0·47
Average cruise speed (ft/s)	620·6	737·4

the climb, and the aircraft does not spend much time at cruise, flight condition at which it is most efficient. However, since the fuel required for the cruise segment varies exponentially with the range, there is an optimum between the two extremes. This optimisation problem is not as practical as the fixed design range problem, since airline operations are heavily constrained by routes, but it is a worthwhile consideration to quantify the benefits of breaking down a long-range flight[7].

Two design problems are solved: one with the cruise Mach number as a design variable, and another with a fixed cruise Mach number. The purpose of the second problem is to investigate how the optimal range varies when a specific cruise speed is required. Table 6 lists the final design variable values as well as additional performance parameters for the two optimal aircraft. A top-view comparison of both aircraft is shown in Fig. 9.

The aircraft optimised with cruise Mach number as a design variable has an optimal range of

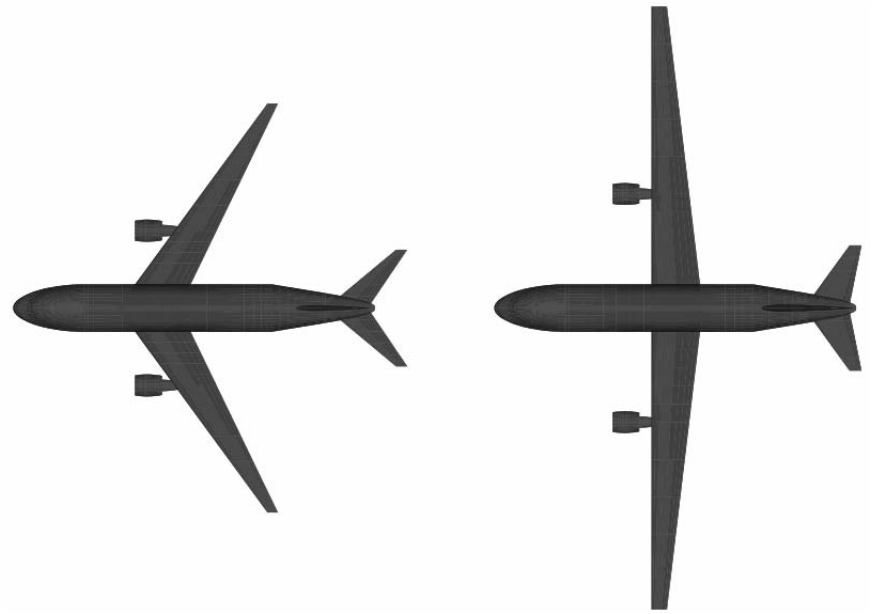

Figure 9. Comparison of narrow-body aircraft optimised for optimal payload-fuel efficiency: Mach = 0.76 (left), Mach = 0·64 (right).

3,433nm and achieves a fuel burn per nautical mile of 7·27lb/nm. The cruising speed of this aircraft is low (Mach = 0·64), which has the primary effect of decreasing the overall propulsive efficiency term in the Breguet range equation. However, the aircraft compensates for this with a high lift-to-drag ratio and efficient engines, which increases its cruise fuel efficiency. The aircraft optimised with a fixed cruise Mach number has an optimal range of 3,040nm and achieves a fuel burn per nautical mile of 7·66lb/nm. To illustrate that the selected ranges are in fact optimal for the given configurations, the payload-fuel efficiency (weight of payload times distance flown divided by the weight of fuel used) is plotted in Fig. 10. As the figure illustrates, the selected ranges for both aircraft are very near their optimal cruise efficiency ranges.

3.1.3 Multi-objective optimisations

A multi-objective optimisation for the narrow-body aircraft with a fixed range is now performed. Two objective functions are considered: the DOC and the mission fuel burn. A multi-objective genetic algorithm is used to solve this problem[38]. Figure 11 shows the Pareto front achieved after 1,000 generations. The figure also shows a planform view of a few of the configurations. In addition to the genetic algorithm results, the plot also contains two optimal configurations from the single objective optimisations performed in Section 3.1.1: the minimum DOC solution as the left-most point, and the minimum fuel burn solution at the far right. The Pareto front illustrates how the planform shape changes between a minimum cost aircraft and a minimum mission fuel burn aircraft. The intermediate solutions have lower wing sweep angles and larger wing spans than the minimum cost aircraft. In addition, the cruise Mach numbers decrease from the high value for the minimum cost aircraft towards a much lower value for the minimum fuel burn aircraft.

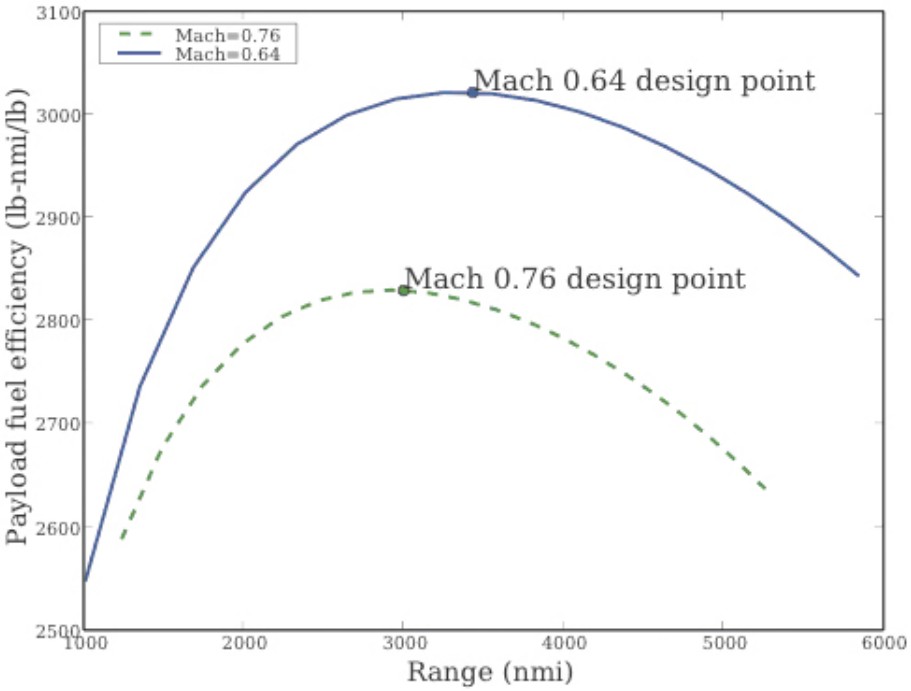

Figure 10. Payload-fuel efficiency of the optimised aircraft.

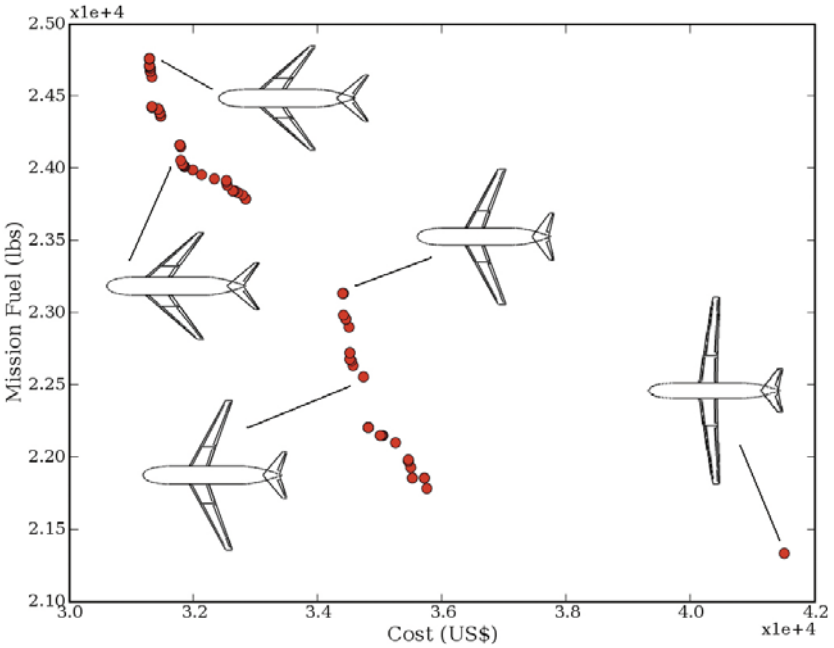

Figure 11. Narrow-body Pareto front for cost and fuel burn.

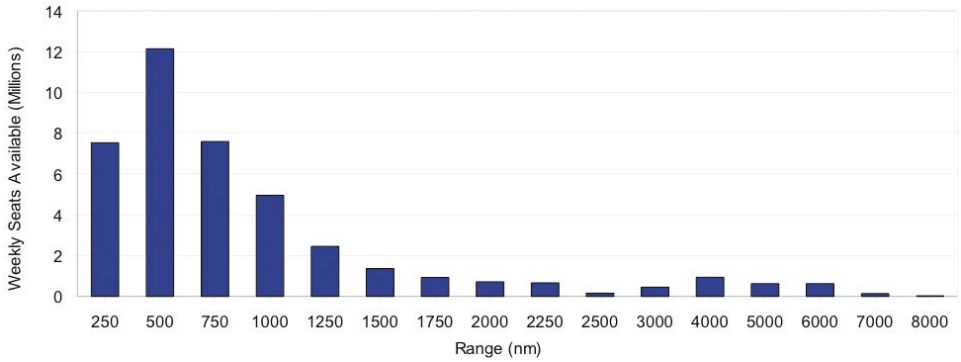

Figure 12. Distribution of flights by length.

3.2 Large aircraft for short ranges

We now explore a concept — large aircraft for short ranges (LASR) — that can reduce the environmental impact of aircraft for a fixed Mach number, range, and technology level[39]. The basic idea behind this type of aircraft is that a reduction in fuel burn can be achieved through the use of a larger and lighter aircraft designed specifically for short ranges and used on heavily trafficked routes. A market analysis performed by Kenway *et al*[39] determined how many existing flights can be replaced by LASRs to determine the overall market size for these aircraft. This market analysis assumed that a LASR aircraft would carry 300 passengers in a two-class configuration. To identify the airline sector to be targeted by LASRs, the services of OAG Aviation[40] were used to determine all the scheduled worldwide flights, considering only one-way single-stage flights with a passenger demand greater than 600 seats per day, and routes where the aircraft size is greater than 100 seats. Figure 12 shows the weekly seats available versus flight range for all flights meeting these requirements. As the figure indicates, more than 90% of all flights are less than 1,500nm.

The flights in this figure represent a significant proportion of aviation greenhouse gas emissions and therefore it is logical to attempt to reduce emissions on these shorter routes. In addition, the majority of aircraft flying these routes have design ranges considerably longer than 1,500nm. Therefore, the benefit of a LASR is evident: if a larger aircraft is designed for shorter ranges, the additional structural weight required for longer flights is removed, making the aircraft lighter, which in turn reduces fuel burn. The LASR could reduce overall emissions by replacing the long-range aircraft operating on short routes and by replacing two or more flights of smaller aircraft with a single flight.

Based on the market analysis, the LASR is required to transport 300 passengers over a 1,500 nmi range. The Airbus A330-200 was selected as the large, long-range reference aircraft, since its two-class seating capacity is 293 seats. The Airbus 330-200 maximum range is 6,400nm. The Airbus A330 Airplane Characteristics for Airport Planning document[41] was used to obtain the reference aircraft weight and performance data listed in Table 7. In addition, the LASR was also compared to a smaller aircraft, the A320-200, which is often used on routes relevant to the LASR.

To validate pyACDT, the weights given by pyACDT for the A320 and the A330 are compared against the actual weights given by Airbus in Table 7. The values inside the brackets are results from pyACDT, and the other values are the actual ones. The results agree well, with a maximum discrepancy of 2%.

For the two reference aircraft, we ran analyses to determine their respective fuel burns at a variety

Table 7
Baseline configurations for LASR studies
(values computed by pyACDT are shown in brackets)

	A330-200	A320-200
Design range (nm)	6,400	3,000
Passengers — 2-class cabin	293	150
Maximum takeoff weight (lb)	513,675 [513,432]	166,447 [168,804]
Operating empty weight (lb)	257,367 [255,628]	90,927 [92,914]
Engine	CF6-80E1	CFM56-5B5
Payload (lb)	62,000	31,500
Fuel (lb)	194,308 [195,804]	44,020 [44,390]

Table 8
LASR performance analysis results for three different missions ranges

Variable	A320-200	A330-200	LASR-15
Passengers — two-class cabin	150	293	293
Design range (nm)	3,000	6,400	1,500
Design Mach	0·76	0·82	0·78
Actual cruise Mach	0·78	0·78	0·78
Cruise altitude (ft)	35,000	39,000	37,370
Payload (lb)	31,500	62,000	62,000
Wing area (ft)	1,318	3,892	2,275
Sea-level static thrust (lb)	25,000	68,000	52,796
Horizontal tail area (ft)	333·7	784·8	497·3
Vertical tail area (ft)	231·5	513·	0 358·4
1,500nm mission			
Take-off weight (lb)	151,217	377,458	306,273
Fuel burn (lb)	19,394	41,334	35,832
Fuel burn (lb/p·nm)	0·086	0·094	0·082
Cruise lift-to-drag ratio	16·2	20·4	18·5
1,000nm mission			
Takeoff weight (lb)	145,529	366,014	296,001
Fuel burn (lb)	13,986	30,450	26,065
Fuel burn (lb/p·nm)	0·093	0·104	0·089
Cruise lift-to-drag ratio	16·0	20·1	18·3
500nm mission			
Takeoff weight (lbs)	139,879	354,649	285,891
Fuel burn (lb)	8,611	19,645	16,451
Fuel burn (lb/p·nmi)	0·115	0·134	0·112
Cruise lift-to-drag ratio	15·6	19·8	18·1

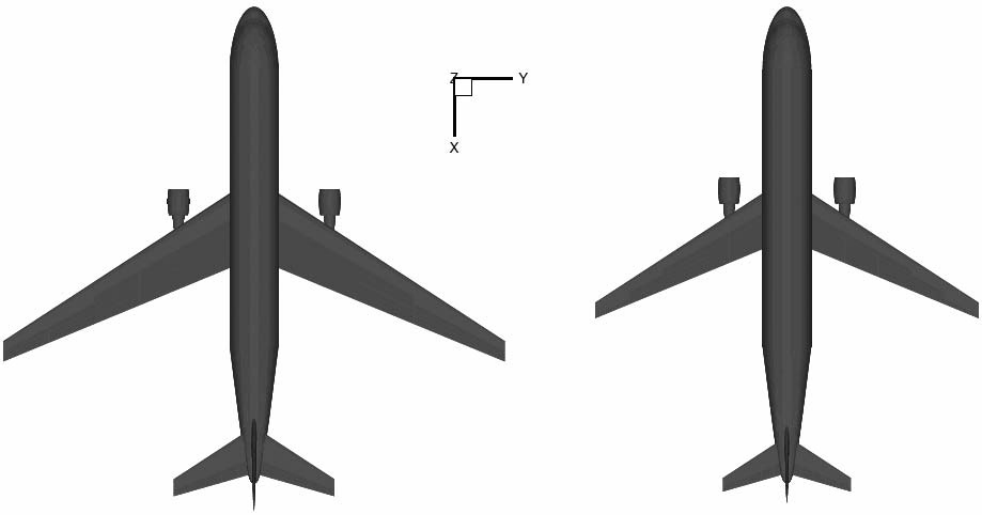

Figure 13. Top view comparison of the A330-200 (left) and LASR (right).

of off-design ranges. In all these analyses, the operational empty weights and payload weights were kept constant. The initial cruise altitude was selected to minimise mission fuel burn for each of the ranges. In addition, the reference aircraft were constrained to have an adequate maximum thrust-to-drag ratio at their initial cruise altitude.

To obtain the LASR design, we optimised an aircraft with the same capacity as the A330-200 but for a shorter range. The optimisation problem was simplified by specifying only five design variables: wing reference area, horizontal tail area, vertical tail area, initial cruise altitude and engine sea-level static thrust. Many of the other design variables, such as engine cycle parameters, were kept constant to ensure that all aircraft had similar technology levels. The cruise Mach number for all aircraft was set to 0·78 to ensure that all aircraft under consideration would maintain similar block times. Table 8 lists performance, weight and aerodynamic data for the two reference aircraft, and the LASR aircraft for flights of 1,500nm, 1,000nm and 500nm.

Based on the data from this table, the LASR can offer up to a 13% reduction in fuel burn per passenger when compared to the A330-200, and a 5% reduction in comparison to two A320-200s, all flying a 1,500nm mission. Figure 13 shows a top-view comparison of the A330-200 and the LASR, where the reduction in wing and tail areas is evident.

4.0 CONCLUSIONS

The environmental impact of aviation is becoming a critical aspect in the design and development of new aircraft. Commercial aviation has become a major mode of transportation and predictions indicate that air travel will continue to grow in the foreseeable future. It is also predicted that the growth in air transport will continue to outpace the development of technologies required to maintain current emissions levels. Therefore, the net result will be an absolute increase in aviation emissions. This is of great concern, not only for local air quality around airports, but also because of the impact that aircraft emissions can have on climate change when emitted at cruise altitudes. This concern is reflected in the agreement that ICAO members reached in 2009 to improve fuel

efficiency by 2% every year through 2020. Additionally, the International Air Transport Association, is aiming for a 50% reduction in carbon emissions relative to 2005 levels by 2050.

The objective of this work was to develop an aircraft environmental design and optimisation framework. The framework — pyACDT — was extended to optimise aircraft configurations for a variety of environmental metrics. These metrics were fuel burn (which is a measure of CO emissions) and LTO NO_X emissions. The aircraft were also optimised for minimum direct operating cost for comparison purposes. All typical aircraft conceptual design disciplines, as well as propulsion and emissions, were integrated into this framework. Since the design space contained many local minima and was also discontinuous, the optimisations were performed using non-gradient based optimisers.

The aircraft optimised for minimum fuel burn exhibited a high aspect ratio wing with lower induced drag. This was achieved without a significant weight penalty by lowering the cruise speed, thus removing the requirement for wing sweep. The decrease in the cruise speed was limited by the propulsive efficiency. The minimum fuel burn aircraft were all designed with high bypass ratio engines and high core pressures and temperatures to achieve high engine efficiency.

The minimum LTO NO emissions aircraft also had a high aspect ratio wing and had the largest wing area when compared to the minimum direct operating cost and minimum fuel burn aircraft. This large wing area was required to compensate for the low-thrust engines. The engines were designed with low thrust levels, high bypass ratios and low core pressures and temperatures. Because of these features, the resulting engines had small core mass flow rates and low NO emissions indices. This aircraft had high direct operating cost due to its low cruise speed, and high fuel burn due to poor engine efficiency.

In an additional study, the mission range was allowed to vary in the minimum fuel burn problem, and the aircraft was optimised for maximum payload-fuel efficiency. The optimal ranges were found to be between 3,000nm and 3,500nm, depending on the cruise Mach number. When the cruise Mach number was added as an additional design variable, the optimal Mach number was 0·64.

In a last study, the possibility of designing large aircraft for short ranges (LASR) was investigated as a way to reduce the overall environmental impact of aviation. It was shown that a reduction in structural weight can be achieved, and consequentially, fuel burn is also decreased. A large aircraft optimised for a 1,500nm range not only outperforms a similarly-sized aircraft designed for longer ranges, but also outperforms two smaller aircraft with the same combined payload.

ACKNOWLEDGEMENTS

The authors would like to thank Gaetan K. W. Kenway, Jason E. Hicken, Nimeesha B. Kuntawala, David W. Zingg and Ross G. McKeand for their contributions in formulating the LASR design optimisation problem, and in interpreting the corresponding results.

REFERENCES

1. SCHAFER, A., and VICTOR, D.G. The past and future of global mobility, *Sci American*, October 1997, pp 36–39.
2. PENNER, J.E., LISTER, D.H., GRIGGS, D.J., DOKKEN, D.J., and MCFARLAND, M. *Aviation and the Global Atmosphere*, 1999, Special report, Intergovernmental Panel on Climate Change.
3. EPA. Evaluation of air pollutant emissions from subsonic commercial jet aircraft, April 1999, Tech Report EPA 420-R-99-013, US Environmental Protection Agency.

4. LE DILOSQUER, M.J.R. The aero engine response to the protection of the global atmosphere, 2001, Gas Turbine Pollutant Emissions, IMechE Seminar Publication, Professional Engineering Publishing Ltd.
5. GARDNER, R.M., ADAMS, K., COOK, T., DEIDEWIG, F., ERNEDAL, S., FALK, R., FLEUTI, E., HERMS, E., JOHNSON, C.E., LECHT, M., NEWON, P., SHMITT, A., VANDERBERGH, C. and VAN DRIMMELEN, R. The ANCAT/EC global inventory of NO emissions from aircraft, *Atmospheric Environment*, 1997, **31**, (12), pp 1751–1766.
6. LEE, D., PITARI, G., GREWE, V., GIERENS, K., PENNER, J., PETZOLD, A., PRATHER, M., SCHUMANN, U., BAIS, A., and BERNTSEN, T. Transport impacts on atmosphere and climate: Aviation, *Atmospheric Environment*, December 2010, **44**, (37), pp 4678-4734.
7. GREEN, J.E. Civil aviation and the environmental challenge, *Aeronaut J*, June 2003.
8. GREEN, J.E. Civil aviation and the environment — the next frontier for the aerodynamicist, *Aeronaut J*, August 2006.
9. WILLIAMS, V., NOLAND, R.B., MAJUMDAR, A., TOUMI, R., OCHIENG, W. and MOLLOY, J. Reducing environmental impacts of aviation with innovative air traffic management technologies, *Aeronaut J*, November 2007, pp 741–749.
10. CHITTICK, I.R. and MARTINS, J.R.R.A. An asymmetric suboptimization approach to aerostructural optimization, *Optimization and Engineering*, March 2009, **10**, (1), pp 133–152.
11. KROO, I.M., ALTUS, S., BRAUN, R.D., GAGE, P.J. and SOBIESKI, I.P. Multidisciplinary optimization methods for aircraft preliminary design, September 1994, AIAA 5th Symposium on Multidisciplinary Analysis and Optimization, Panama City Beach, FL, AIAA 1994-4325.
12. MALONE, B. and MASON, W. Multidisciplinary optimization in aircraft design using analytic technology models, *J Aircr* March-April 1995, **32**, (2), pp 431–438.
13. MARTINS, J.R.R.A., ALONSO, J.J. and REUTHER, J.J. High-fidelity aerostructural design optimization of a supersonic business jet, *J Aircr*, 2004, **41**, (3), pp 523–530.
14. ANTOINE, N.E. and KROO, I.M. Aircraft optimization for minimal environmental impact, *J Aircr*, 2004, **41**, (4), pp 790–797.
15. ANTOINE, N.E. and KROO, I.M. Framework for aircraft conceptual design and environmental performance studies, *AIAA J*, October 2005, **43**, (10), pp 2100–2109.
16. SCHWARTZ, E. and KROO, I.M. Aircraft design: Trading cost and climate impact, January 2009, 47th AIAA Aerospace Sciences Meeting, Orlando, FL, AIAA 2009-1261.
17. DIEDRICH, A., HILEMAN, J., TAN, D., WILLCOX, K. and SPAKOVSZKY, Z. Multidisciplinary design and optimization of the silent aircraft, January 2006, 44th AIAA Aerospace Sciences Meeting and Exhibition, Reno, NV.
18. JONES, A.R., WILLCOX, K.E. and HILEMAN, J.I. Distributed multidisciplinary optimization of aircraft design and takeoff operations for low noise, April 2006, 48th AIAA/ASME/ASCE/AHS/ASC Structures, Structural Dynamics, and Materials Conference, Honolulu, HI, AIAA 2007-1856.
19. LEIFSSON, L.T. Multidisciplinary Design Optimization of Low-Noise Transport Aircraft, 2005, PhD thesis, Virginia Polytechnic Institute and State University.
20. PEREZ, R.E. and MARTINS, J.R.R.A. pyACDT: An object-oriented framework for aircraft design modelling and multidisciplinary optimization, September 2008, 12th AIAA/ISSMO Multidisciplinary Analysis and Optimization Conference, Victoria, BC, Canada.
21. RAYMER, D. *Aircraft Design: A Conceptual Approach*, Third edition, 1999, AIAA Education Series, American Institute of Aeronautics and Astronautics, Washington, DC, USA.
22. ROSKAM, J. *Airplane Design*, Second edition, Vol 1-8, 1998 DARCorporation, Ottawa, KS, USA.
23. TORENBEEK, E. *Synthesis of Subsonic Airplane Design*, Sixth edition, 1990, Delft University Press and Kluwer Academic Publishers.
24. CHAI, S., CRISAFULLI, P. and MASON, W. Aircraft center of gravity estimation in conceptual and preliminary design, P, September 1995, 1st Aircraft Engineering, Technology, and Operations Congress, Los Angeles, CA, AIAA 1995-3882.
25. SCHAUFELE, R.D. *The Elements of Aircraft Preliminary Design*, 2007, Aries Publications.
26. JANSEN, P., PEREZ, R.E. and MARTINS, J.R.R.A. Aerostructural optimization of nonplanar lifting surfaces, *J Aircr*, 2010, **47**, (5), pp 1491–1503.
27. ANONYMOUS. Increment in aerofoil lift coefficient at zero angle of attack and in maximum lift coefficient due to deployment of various leading-edge high-lift devices at low speeds, December 1994, Tech Report 94027, ESDU.
28. ANONYMOUS. Increments in aerofoil lift coefficient at zero angle of attack and in maximum lift coefficient due to deployment of a double-slotted or triple-slotted trailing-edge flap, with or without a leading-edge high-lift device, at low speeds, April 1995, Tech Rep 94031, ESDU.
29. ANONYMOUS. Maximum lift of wings with leading-edge devices and trailing-edge flaps deployed, November 1995, Tech Report 92031, ESDU.

30. ANONYMOUS. Maximum lift of wings with trailing-edge flaps at low speeds, August 1995, Tech Report 91014, ESDU.
32. MARCH, A. Influence of Low-speed Aerodynamic Performance on Airport Community Noise, 2008, Master's thesis, Massachusetts Institute of Technology.
32. HENDERSON, R. Multidisciplinary Design Optimization of Airframe and Engine for Emissions Reduction, 2009, Master's thesis, University of Toronto Institute for Aerospace Studies, Toronto, ON, Canada.
33. ANTOINE, N.E. and KROO, I.M. Framework for aircraft conceptual design and environmental performance studies, *AIAA J*, October 2005, **43**, (10), pp 2100–2109.
34. LUKACHKO, S.P. and WAITZ, I.A. Effects of engine aging on aircraft NOx emissions, 1997, ASME International Gas Turbine and Aero-Engine Congress and Exhibition.
35. LEFEBVRE, A. H. *Gas Turbine Combustion*, Second edition, 1998, Taylor and Francis, Ann Arbor, MI, USA.
36 PEREZ, R.E., JANSEN, P. W. and MARTINS, J.R.R.A. pyOpt: a Python-based object-oriented framework for non-linear constrained optimization, *Structural and Multidisciplinary Optimization*, 2011 (In press).
37. NOCEDAL, J. and WRIGHT, S.J. *Numerical Optimization*, 2006, Second edition, Springer.
38. DEB, K., PRATAP, A., AGARWAL, S. and MEYARIVAN, T. A fast and elitist multi-objective genetic algorithm: NSGA-II, 2000, Tech Report 200001, Kanpur Genetic Algorithms Laboratory, Indian Institute of Technology, Kanpur.
39. KENWAY, G.K., HENDERSON, R., HICKEN, J.E., KUNTAWALA, N B., ZINGG, D.W., MARTINS, J.R.R.A. and MCKEAND, R.G. Reducing aviation's environmental impact through large aircraft for short ranges, January 2010, 48th AIAA Aerospace Sciences Meeting and Exhibitition, Orlando, FL, AIAA 2010-1015.
40. ANONYMOUS. OAG aviation, http://www.oagaviation.com/.
41. ANONYMOUS. A330 airplane characteristics for airport planning ac, January 1993, Tech report, Airbus.